

1 ***pyQCM-BraTaDio: A tool for visualization, data mining, and modelling of Quartz crystal***  
2 ***microbalance with dissipation data***

3  
4 Brandon M. Pardi, Materials Science and Engineering, University of California Merced, 5200 N.  
5 Lake Rd, 95344, Merced, CA, USA, [bpardi@ucmerced.edu](mailto:bpardi@ucmerced.edu), ORCID: 0000-0001-6483-9858

6 Syeda Tajin Ahmed, Materials Science and Engineering, University of California Merced, 5200  
7 N. Lake Rd, 95344, Merced, CA, USA, [sahmed65@ucmerced.edu](mailto:sahmed65@ucmerced.edu), ORCID: 0000-0002-2719-  
8 9641

9 Silvia Jonguitud Flores, Instituto de Física, Universidad Autónoma de San Luis Potosí, San Luis  
10 Potosí 78000, Mexico, [silviac@ifisica.uaslp.mx](mailto:silviac@ifisica.uaslp.mx), ORCID: 0009-0005-4841-4901

11 Warren Flores, Materials Science and Engineering, University of California Merced, 5200 N.  
12 Lake Rd, 95344, Merced, CA, USA, [svandyke-flores@ucmerced.edu](mailto:svandyke-flores@ucmerced.edu), ORCID: 0009-0001-  
13 1462-4688

14 Laura L.E. Mears, Institute of Applied Physics, Technische Universitaet Wien, Vienna  
15 1030, Austria, [mears@iap.tuwien.ac.at](mailto:mears@iap.tuwien.ac.at), ORCID: 0000-0001-7558-9399

16 Bernardo Yáñez Soto, Instituto de Física, Universidad Autónoma de San Luis Potosí, San Luis  
17 Potosí 78000, Mexico, [byanez@ifisica.uaslp.mx](mailto:byanez@ifisica.uaslp.mx), ORCID: 0000-0002-4273-6513

18 Roberto C. Andresen Eguiluz, Materials Science and Engineering, Health Sciences Research  
19 Institute, University of California Merced, 5200 N. Lake Rd, 95344, Merced, CA, USA,  
20 [randreseneguiluz@ucmerced.edu](mailto:randreseneguiluz@ucmerced.edu), ORCID: 0000-0002-5209-4112

21 **Abstract**

22 Here, we present a Python based software that allows for the rapid visualization, data mining, and  
23 basic model applications of quartz crystal microbalance with dissipation data. Our implementation  
24 begins with a Tkinter GUI to prompt the user for all required information, such as file  
25 name/location, selection of baseline time, and overtones for visualization (with customization  
26 capabilities). These inputs are then fed to a workflow that will use the baseline time to scrub and  
27 temporally shift data using the Pandas and Numpy libraries and carry out the plot options for  
28 visualization. The last stage consists of an interactive plot, that presents the data and allows the  
29 user to select ranges in Matplotlib-generated panels, followed by application of data models,  
30 including Sauerbrey, thin films in liquid, among others, that are carried out with NumPy and SciPy.  
31 The implementation of this software allows for simple and expedited data analysis, *in lieu* of time  
32 consuming and labor-intensive spreadsheet analysis.

33 **Keywords**

34 *Quartz Crystal Microbalance with Dissipation; QCM-D; Sauerbrey; thin film in liquid.*

35

36 **Metadata**

37

Nr	Code metadata description	<b>Please fill in this column</b>
C1	Current code version	<i>Version b.1.1</i>
C2	Permanent link to code/repository used for this code version	<a href="https://gitlab.com/randresen/BraTaDiO">https://gitlab.com/randresen/BraTaDiO</a>
C3	Permanent link to reproducible capsule	<i>None (UI based software)</i>
C4	Legal code license	<i>MIT License</i>
C5	Code versioning system used	<i>git</i>
C6	Software code languages, tools and services used	<i>Python (Numpy, Tkinter, Matplotlib, Scipy, Pandas)</i>
C7	Compilation requirements, operating environments and dependencies	<i>README.md file in GitLab repository</i>
C8	If available, link to developer documentation/manual	<i>README.md file in GitLab repository</i>
C9	Support email for questions	<a href="mailto:bpardi@ucmerced.edu">bpardi@ucmerced.edu</a> <a href="mailto:randreseneguiluz@ucmerced.edu">randreseneguiluz@ucmerced.edu</a>

38

39 **1. Motivation and significance**

40 Quartz crystal microbalance with dissipation (QCM-D) is an acoustic-based, surface sensitive  
41 technique that measures small mass changes and energy losses, in real time, at the surface of a  
42 sensor. The sensors are commonly fabricated from a piezoelectric material, such as quartz, which

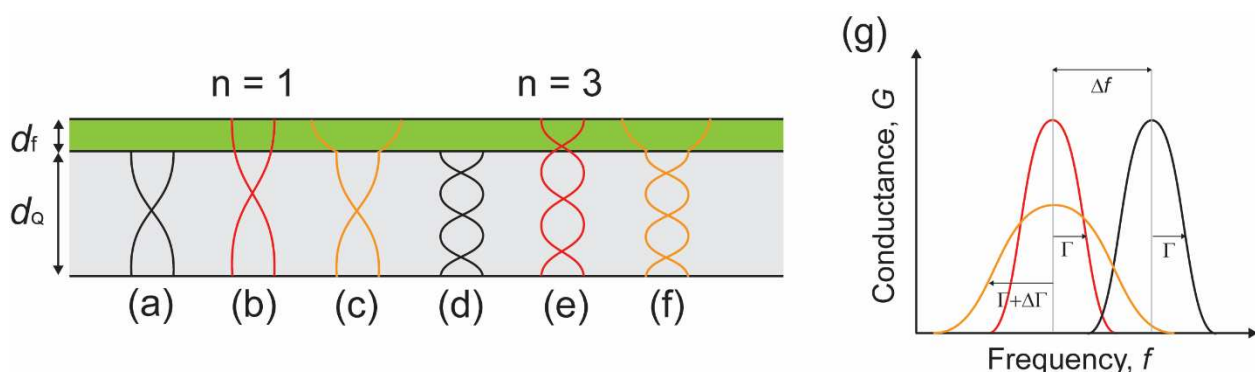


**Figure 1.** (a) and (d) Standing wave of overtone orders  $n = 1$  and  $n = 3$  across the thickness of the sensor,  $d_Q$ . (b) and (e) Increased sensor thickness due to analyte film decreases resonance frequency. (c) and (f) When the analyte film is softer than the sensor, the interface generates a distortion to the standing wave, and the frequency shift becomes proportional to the mass, rather than the thickness. (g) Frequency and bandwidth shifts,  $\Delta f$  and  $\Delta\Gamma$ , respectively, are used to measure changes in film thickness  $d_f$  and energy losses.

43 allows thickness-shear of the sensors at its resonance frequencies by applying an alternating  
44 electric field. The most common cut of quartz crystals for QCM-D applications is the AT-cut, as it  
45 has excellent frequency-temperature characteristics.<sup>1</sup> For these sensors, there are  $n$  number of  
46 acoustic modes, referred to here as overtones or overtone order, that can be approximated as  
47 standing waves perpendicular to the crystal surface with negligible longitudinal wave propagation.

48 The penetration depth of a 5 MHz shear wave in water is approximately  $\delta \approx 250$  nm for the  
49 fundamental overtone and  $\delta \approx 70$  nm for the 13<sup>th</sup> overtone,<sup>2,3</sup> making QCM-D a surface-sensitive  
50 instrument. For small films formed by analytes at the surface of the sensor, the resonance  
51 frequency  $f$  is inversely proportional to the total thickness of the plate. That is, the effective  
52 thickness  $d_{\text{eff}} = d_Q + d_f$  of the sensor increases with increasing amount of analyte coupled to the  
53 sensor surface, decreasing its resonance frequency  $f$ . This relationship was first identified by  
54 Sauerbrey,<sup>4</sup> and is schematized in Figure 1. When the forming film is rigid or very thin (and  
55 homogeneous and continuous), the film-sensor interface does not change the bandwidth ( $\Delta\Gamma = 0$ ). However, if the forming films are viscoelastic (or heterogeneous or discrete), the shift or  
56 change in frequency  $\Delta f$  is coupled with a change in bandwidth as well ( $\Delta\Gamma \neq 0$ ), and the ideal  
57 inverse linear relationship between changes in thickness and changes in frequency no longer  
58 apply.<sup>5</sup>

60 QCM-D has gained popularity in many different scientific fields due to its experimental simplicity  
61 and versatility. QCM-D (or just QCM if not quantifying energy losses) can be combined with a  
62 variety of instruments for *in situ* complementary measurements, such as atomic force microscopy  
63 (AFM),<sup>6</sup> microtribometry,<sup>7</sup> surface plasmon resonance (SPR),<sup>8</sup> or electrochemistry,<sup>9</sup> among  
64 others. However, one drawback rests in linking experimental conditions, understanding  
65 relationships between changes in frequency  $\Delta f$  and changes in bandwidth  $\Delta\Gamma$ , to meaningful  
66 models. For example, films can be laterally homogeneous or heterogeneous, isotropic or  
67 anisotropic, the dissipation can take place inside the film or at a particle-surface region,  
68 continuous or discrete, and the bulk solution can be Newtonian or non-Newtonian. All these  
69 conditions will dictate the applicability of specific models. In a collection of works,<sup>10-20</sup> Johannsmann  
70 and co-workers have developed, refined, and summarized qualitative and  
71 quantitative approaches for the analysis and interpretation of QCM-D data, which the reader is  
72 encouraged to review. Kanazawa and Gordon<sup>21,22</sup> derived a simple relationship which expresses  
73 the change in frequency  $\Delta f$  in contact with a fluid only in terms of the material parameters of the  
74 fluid (*i.e.*, density  $\rho_F$  and viscosity  $\mu_F$ ) and the quartz crystal (*i.e.*, density  $\rho_Q$  and shear modulus  
75  $\mu_Q$ ). The relationship is valid for semi-infinite viscoelastic media. Du and Johannsmann<sup>12</sup> derived

76 the elastic compliance  $J'_f$  of a viscoelastic film deposited on a quartz crystal surface in a liquid  
77 environment from the ratio of bandwidth shift  $\Delta\Gamma$  and frequency shift  $\Delta f$ . Voinova *et al.* derived the  
78 general solution describing the dynamics of two-layer viscoelastic materials of arbitrary thickness  
79 deposited on a solid (the quartz crystal) surface in a fluid environment.<sup>23</sup> This relationship can be  
80 used for QCM-D measurements of layered

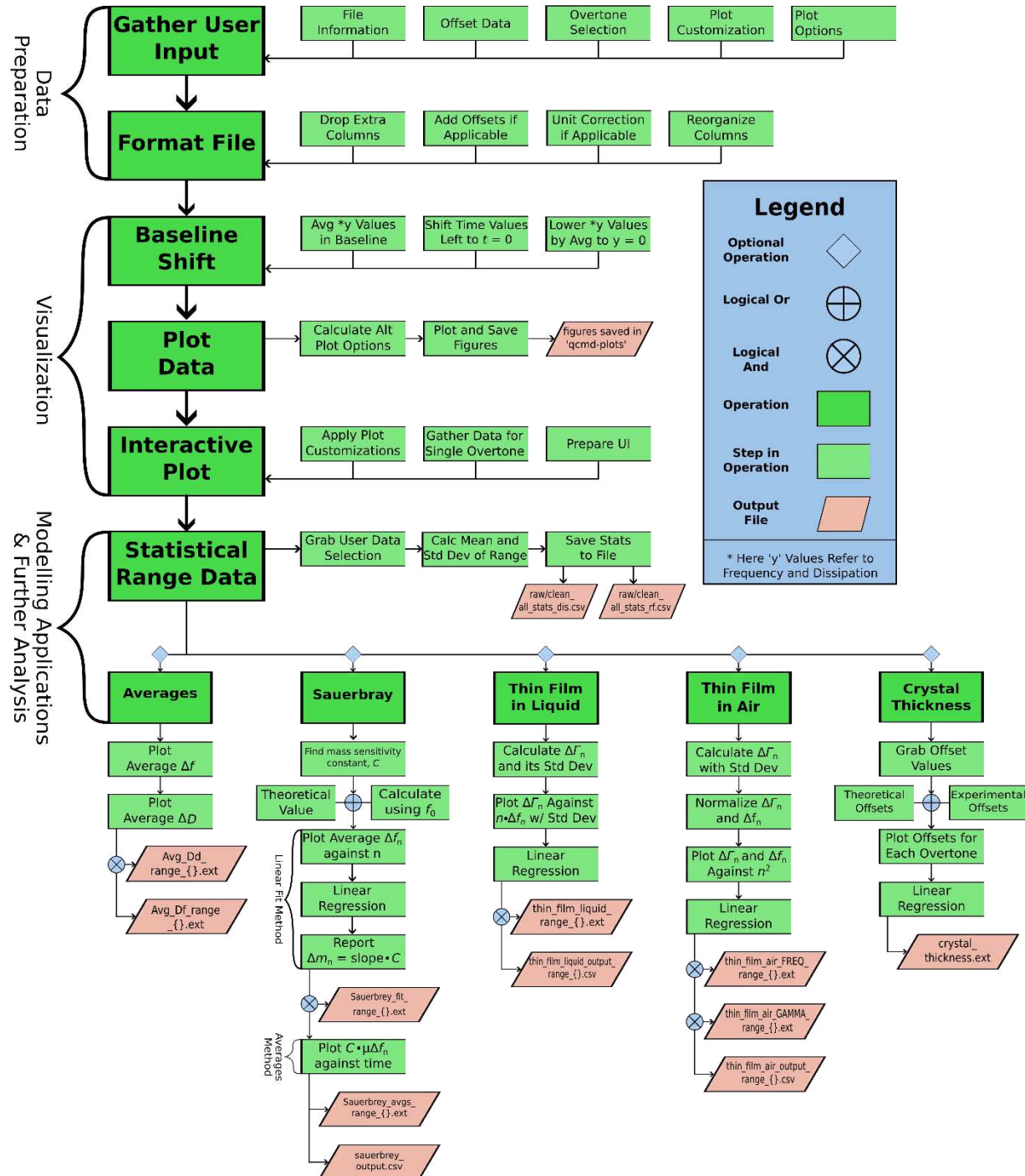


**Figure 2.** pyQCM-BraTaDiO workflow and structure of operations. Beginning with data preparation, pyQCM-BraTaDiO takes in the input fields specified by the user in the UI, and formats the file dependent on the experimental apparatus used to record the data. Once data is prepared, it is then visualized. This includes shifting data by the baseline, computing alternate plot options, saving figures, and generating the interactive plot. The optional modelling and further analysis layer can commence after visualization. This starts with the user making selections in the interactive plot and basic statistical calculations being applied on those selections, and ends with the execution of various available models for the data previously selected.

82 structures, such as protein films adsorbed from solution (the analyte) onto the surface or swelling  
83 and deswelling of polymer brushes. Despite the relative simplicity with which QCM-D operates  
84 and its versatility, it becomes clear that quantitative results are non-trivial to obtain and require  
85 careful analysis.

86 In any QCM-D experiment, real-time monitoring of sensor surface-environment generates large  
87 volumes of data entries. Packages used to collect data do not typically possess straightforward  
88 data visualization, data mining capabilities, and basic model applications. Furthermore, programs  
89 associated with QCM-D data collection and analysis are often proprietary with limited access.  
90 There are other open source packages, such as RheoQCM<sup>24</sup> and pyQTM,<sup>25</sup> however, they focus  
91 on data modelling rather than data mining. Here, we present an intuitive Python-based, open-  
92 source software that is QCM-D manufacturer agnostic of multi-harmonic collecting systems for  
93 (1) simple and fast data visualization and interaction, (2) data mining and reduction, (3) crystal  
94 thickness calibration, and (4) basic model applications. The supported models include (i)  
95 Sauerbrey, for rigid thin films, (ii) Johannsmann, for viscoelastic thin film in a Newtonian liquid,  
96 and (iii) quartz crystal thickness determination. Lastly, we validate the software by visualizing and  
97 applying models to data collected with two commercial multi-harmonic QCM-D systems.

98 **2. Software description**

99 To perform the various levels of data visualization, applying models, and fitting possible with  
100 pyQCM-BraTaDio tool, it is crucial for the input data files to have the correct data structure and  
101 file extensions, depending on the source system. Supported data structures at the time of writing  
102 include QSense, QCM-I, and openQCM-D Next. Raw data is required to be exported to one of  
103 the following formats: \*.txt, \*.csv, \*.xls, \*.xlsx, and \*.xlsm. The format structure for the data that  
104 each system generates, and more importantly, format structure that the pyQCM-BraTaDio tool  
105 converts to for further operations are detailed in the SI Input Data Structure section.

106 **2.1. Software architecture:**

107 pyQCM-BraTaDio is a Python package implemented in Python 3.10.5, intended to be used as a  
108 data visualization (plotting), experimental data mining, and basic model application tool for multi-  
109 harmonic QCM-D experimental data. It operates by following the workflow and file database  
110 organization shown in Figure 2. The main steps of the workflow are the generation of multiple  
111 data frames from the input file, customization of the plotting properties, selection of overtone  
112 orders ( $n$ ) for display and analysis, selection and labelling of data ranges, calculation of average  
113 frequencies ( $f_n$ ) and dissipations ( $D_n$ ), average change in frequencies ( $\Delta f_n$ ) and average change

114 in dissipations ( $\Delta D_n$ ) of  
 115 selected and labelled  
 116 data ranges, with  
 117 corresponding standard  
 118 deviations, and model  
 119 (e.g., Sauerbrey mass,  
 120  $m_{\text{Sauerbrey}}$ , shear-  
 121 dependent compliance of  
 122 thin films,  $J_f'$ , and quartz  
 123 crystal thickness  
 124 estimation,  $h_q$ ) selection.

125 Selection of multiple data  
 126 ranges is possible, for  
 127 example, for selecting  
 128 ranges corresponding to  
 129 double-layers or buffer washes.

130 pyQCM-BraTaDio generates several output files. All generated plots are saved in the “qcmd-plots”  
 131 directory and model application plots saved in a subdirectory within named “modelling” with the  
 132 selected output format (e.g., PNG, TIFF, or PDF). Calculated averages and standard deviations  
 133 of selected ranges using the interactive plot are saved in a \*.csv file for the chosen overtone order  
 134 frequencies and dissipations in the “selected\_ranges” directory. pyQCM-BraTaDio includes  
 135 python functions to read, compare, and statistically analyze the resulting \*.csv files, detailed in  
 136 the “Comparison of experimental data to theoretical models” section. Alternatively, the resulting  
 137 files can be opened with standard text editors or data analysis tools such as Excel or Origin for  
 138 further analysis.

139 pyQCM-BraTaDio utilizes several well-established open-source python packages. Most notably,  
 140 Pandas,<sup>26</sup> Numpy,<sup>27</sup> for a variety of computational tasks, Tkinter for the interactive plotting engine  
 141 and application user interface (UI),<sup>28</sup> Matplotlib<sup>29</sup> for the display of scatter plots and models and  
 142 interactive plot interface, and SciPy<sup>30</sup> for much of the model application capabilities. Pandas is a  
 143 package providing flexible data structures to make working with relational or labelled data easy.  
 144 It provides an intuitive way of working with data from spreadsheets, interacting with it with code.  
 145 It is a high level, fundamental building block data for analysis in Python. NumPy is another core  
 146 building block, as all the other libraries used rely on it as well. NumPy is used in almost every field



**Figure 3.** User interface of pyQCM-BraTaDio. (1) Initialization conditions, (2) selection of frequencies and dissipation for data mining, visualization, and modeling, (3) interactive plotting options for data range selection, and (4) selection of plotting options and modeling.

147 of science and engineering in Python, containing multidimensional array and matrix data  
148 structures, allowing for easy operations on complexly related data. The number of available  
149 operations is enormous, and they are also guaranteed an optimized runtime. Matplotlib is the core  
150 visualization tool used for this software. It is a comprehensive library for designing and efficiently  
151 plotting static, animated, and interactive plots in Python. SciPy is the final pivotal library for this  
152 software. It provides highly optimized fundamental algorithms for model applications and analysis,  
153 such as integration, interpolation, statistics, and more. SciPy is the library behind our model  
154 application routines. It is a very powerful tool that is relatively simple to use in conjunction with  
155 our other libraries.

156 Our implementation begins with a Tkinter GUI to prompt the user for all required and optional  
157 information, such as file name/location, baseline time, which overtones to plot, and any additional  
158 data plot options. These inputs are then fed to an analysis workflow that will use the baseline time  
159 to scrub data using the Pandas library and carry out the plot options. The platform, most  
160 importantly, incorporates an interactive plot, that allows the user to choose the range of  
161 experimental data over time to calculate data averages and standard deviations. These will be  
162 used as input for the various model applications.

163 The implementation of this software allows for expedited data mining and analysis, *in lieu* of time  
164 consuming and laboring spreadsheet analysis needed for one experiment.

## 165 **2.2. Software functionalities**

166 The interaction with pyQCM-BraTaDio is via a GUI, which allows the user to interact with the  
167 software with minimal to no console interaction. The main window is organized into four main  
168 regions, shown in Figure 3. These regions are (1) initialization conditions, (2) selection of  
169 frequencies and dissipation for data mining, visualization, and model application purposes, (3)  
170 interactive plots for data mining, and (4) selection of plotting options and models.

### 171 **2.2.1 Entering data file information.**

172 In region (1) from the main GUI shown in Figure 3, the user loads the relevant file in any of the  
173 supported formats: \*.txt, \*.csv, \*.xls, or \*.xlsx, and indicates the data structure by selecting the  
174 multi-harmonic instrument that generated the data. Next, the '*relative baseline time*' ('*absolute*  
175 *baseline time*' for openQCM Next) refers to the beginning ( $t_0$ ) and end ( $t_f$ ) of what will be  
176 considered the experimental baseline. For example, if the file contains an air-to-liquid transition,

177 followed by an equilibration time, the relative baseline time will consist of  
178 the last minutes of the equilibration time. pyQCM-BraTaDio calculates  
179 the average  $\Delta f_n$  and average  $\Delta D_n$  of all datapoints within the selected  
180 range (between  $t_0$  and  $t_f$ ) and uses those averages to set the reference  
181 (i.e.,  $\Delta f_n \approx 0$  Hz and  $\Delta D_n \approx 0$ ).

182 The user is next asked to indicate usage of either theoretical or  
183 experimental offset values for resonant frequency calculations. Selecting  
184 theoretical uses resonant frequency values for 5 MHz AT-cut quartz  
185 crystals outlined in SI Table 1, selecting offset will lead to two potential  
186 workflows. If the user has selected QCM-I, the offset values are  
187 automatically taken from the user-inputted baseline time frame. If  
188 QSense is selected, the user will be prompted to either enter values in  
189 the window shown in Figure 4 or edit the  
190 'COPY\_PASTE\_OFFSET\_VALUES\_HERE.csv' file in the 'offset\_data'  
191 directory. It should be noted that these offset values are not required for  
192 basic visualization purposes, but model application functions will not be viable as they rely on the  
193 resonant frequency values for calculation. It is necessary to keep in mind that the typically  
194 reported values of dissipation  $D_n$  are related to bandwidth  $\Gamma_n$  by:<sup>22</sup>

195 
$$D_n = \frac{\Gamma_n}{f_n} \quad (1)$$

196 where  $D_n$  is the dissipation of order  $n$ ,  $\Gamma_n$  is the bandwidth of order  $n$ , and  $f_n$  is the resonance  
197 frequency of order  $n$ .

198 Finally, it is necessary to submit input by clicking the 'Submit file information'. The user also has  
199 the capability of personalizing the plotting aesthetics, such as size and font type for axis titles, x  
200 and y plotting ranges, selecting colors for data, among others. These options are described in the  
201 Customize Plot Options section in the SI.

## 202 **2.2.2 Data selection for visualization, mining, and analysis**

203 The data selection region allows the users to choose the frequencies and dissipations from  
204 specific overtones for data mining, visualization, and model application purposes. pyQCM-  
205 BraTaDio works with overtones  $n = 1, 3, 5, 7, 9, 11, 13$ . It is also here where the user selects to  
206 work with the raw, full data range (i.e., from the first to last data point acquired) or with the

Offset Data	
Input offset frequency values here these values will be used for modeling purposes	
Supports exponential format: i.e. 2.5e-6 or 1.34e7	
1st frequency	4960883.202
1st dissipation	0.000186857
3rd frequency	14866043.56
3rd dissipation	9.94E-05
5th frequency	24773492.76
5th dissipation	7.85E-05
7th frequency	34679594.69
7th dissipation	6.72E-05
9th frequency	44586432.02
9th dissipation	6.16E-05
11th frequency	54493087.56
11th dissipation	5.71E-05
13th frequency	64400340.95
13th dissipation	5.47E-05

**Clear all selections**

**Confirm selections**

**Figure 4.** Input window for calibration obtained frequency and dissipation values (sometimes referred to as offset values).

207 experimental data (*i.e.*, from a predetermined data point to the last data point acquired) and taking  
208 the changes in frequencies ( $\Delta f_n$ ) and dissipations ( $\Delta D_n$ ).

209 **2.2.3 Interactive plots**

210 To facilitate the procedure of data mining, that is, selection of frequency  
211 and dissipation ranges for time ranges of interest, it is possible to interact  
212 with the data via the interactive plots in two ways. First, the user is  
213 required to select the *Interactive plot* option under either *Plot raw data* (*f*  
214 and *D*) or *Plot shifted data* ( $\Delta f$  and  $\Delta D$ ). Next, it is necessary to designate  
215 one of the available overtones for data visualization (*e.g.*,  $n = 3$  in Figure  
216 5) and a label to the data range (*e.g.*, After\_PBS in Figure 5). Note that  
217 even though one overtone is selected for visualization, operations done  
218 in the interactive plot will apply to all overtones selected in the GUI. Lastly,  
219 to enable the interactive plot, the user must check the box labelled  
220 ‘enable interactive plot’. The interactive plot will then display *f* and *D* or  $\Delta f$   
221 and  $\Delta D$ , depending on the selection. Figure 6 shows the latter case.

222 The interactive plot window consists of 5 panels, an input text field to numerically provide a time  
223 range of interest in user-predefined units (default is seconds), Figure 6(a). The time range will be  
224 highlighted in the

225 frequency, Figure 6(b), (b)

226 and dissipation, Figure

227 6(d), interactive plots.

228 Alternatively, the user can

229 select a range by clicking

230 and holding the left mouse

231 button in either direction of

232 the frequency or

233 dissipation interactive

234 plots. The input text field

235 will be updated and

236 display the time limits of

237 the selection. Interactive

238 frequency and interactive

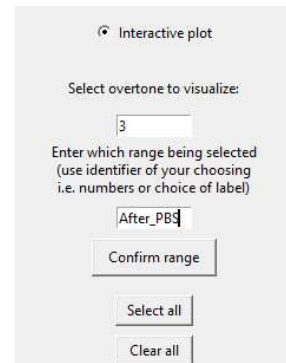


**Figure 5.** Activating the interactive plot option requires to select an overtone and assign a label or identifier for data mining.

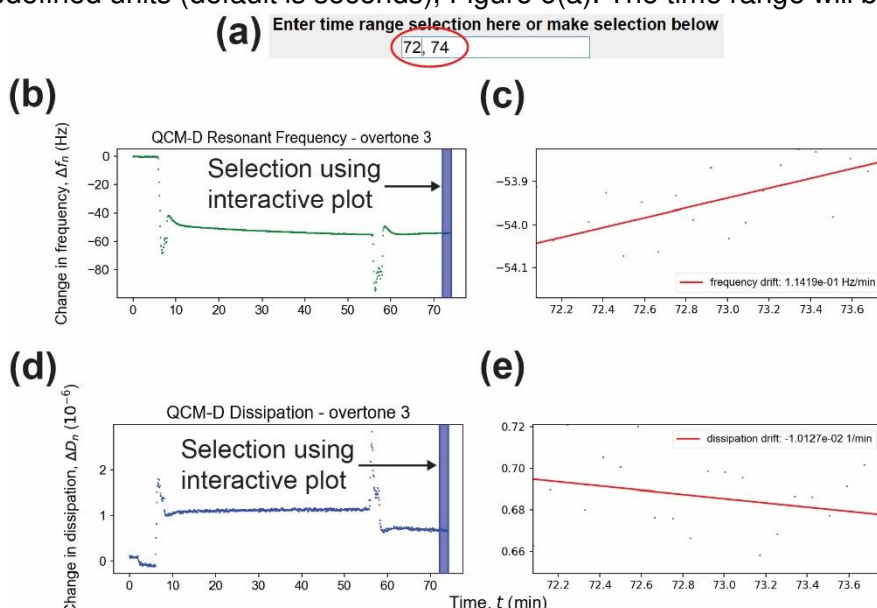


**Figure 6.** (a) Input line for time range selection, (b) change in frequency interactive plot, (c) zoomed-in region from the change in frequency interactive plot and frequency drift, (d) change in dissipation interactive plot, and (e) zoomed-in region from the change in dissipation interactive plot and dissipation drift.

239 dissipation plots are coupled, that is, same time ranges will be applied to frequency and  
240 dissipation channels. The plots shown in Figures 6(c) and (e) display the selected range only and  
241 calculated drift by applying a linear regression. For frequency, it will be in units of Hz over time,  
242 and numerical value over time for the dissipation (*i.e.*, seconds, minutes, or hours, depending on  
243 the selected unit under the *Customize plot options* menu). pyQCM-BraTaDio will compute the  
244 average and standard deviation of the data points contained within the selected range for each  
245 overtone selected, every time a selection is made. The range can be moved and adjusted as  
246 needed, and the new average and standard deviation computed will be updated each time.  
247 Repeating the process overwrites the previously saved average and standard deviation for that  
248 specific range identifier. The average and standard deviation will be calculated for all selected  
249 overtones (all  $f_n$ ,  $\Delta f_n$ ,  $D_n$ , and  $\Delta D_n$ ) in a file contained in the *selected\_ranges* directory. Details on  
250 the file structure can be found in the *Description of directories and output files* section of the  
251 Supporting Information.

252 Changing the range identifier signals to pyQCM-BraTaDio that a new experimental step has been  
253 selected and averages and standard deviations will be saved in new fields (instead of overwriting  
254 the previously stored values). Note that when a new range is selected, data for previous ranges  
255 will remain untouched and new selections will only update for the currently identified range. This  
256 data will remain untouched until the user clicks the '*Clear saved ranges*' button in column 4, which  
257 is recommended when switching to new experimental data, or using different models.

258 It should be noted that depending on the data file size, combined with computational power,  
259 processing time can vary between a fraction of a second to a few seconds. Faster processing  
260 times were demonstrated using a Ryzen 9 5900X 12 core (24 threads) processor at 4.5GHz with  
261 32 GB of RAM, while the lower end of software execution speed was using a more conventional  
262 computer, consisting of an Intel i7-10510U 4 core (8 thread) processor at 1.8 GHz and 16 GB of  
263 RAM.

## 264 **3. Illustrative examples**

### 265 **3.1 Plot options**

266 As in any experimentally obtained data, visual inspection is crucial for an initial assessment of  
267 baseline stability, anomalies, such as presence of undesired air bubbles, leaks, signal loss,  
268 among others. Two basic visualization options are implemented in the pyQCM-BraTaDio tool: (i)  
269 a full data range visualization referred here as raw data, Figure 7, and (ii) the experimental data,  
270 referred here as shifted data, Figure 8. For these options, the user can select the overtone order(s)

271 to visualize the frequency and  
272 dissipation in various plotting  
273 formats. Figure 7(a) and 7(b)  
274 show the absolute frequency  $f_n$   
275 and dissipation  $D_n$  as a function  
276 of time  $t$  for  $n = 1, 3, 5, 7, 9, 11,$   
277 and 13 for a BSA solution  
278 absorbing to a gold substrate,  
279 as described in the SI under  
280 'Model experiments' section  
281 using a QCM-I unit. SI Figures 4 and 5 show similar plots to Figures 7 and 8 for an identical  
282 experiment performed using QSense. When plotting the raw data (absolute frequency and  
283 dissipation values), only the *Plot raw data* option with at least one overtone must be selected.

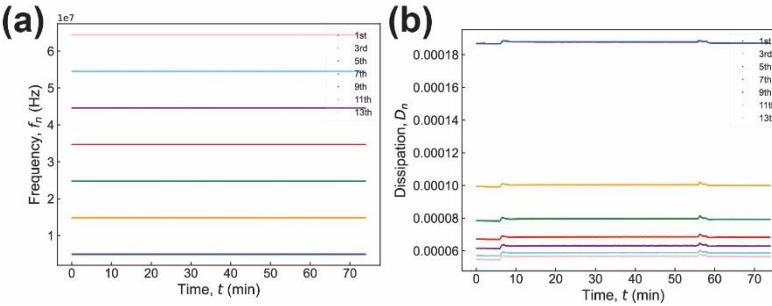
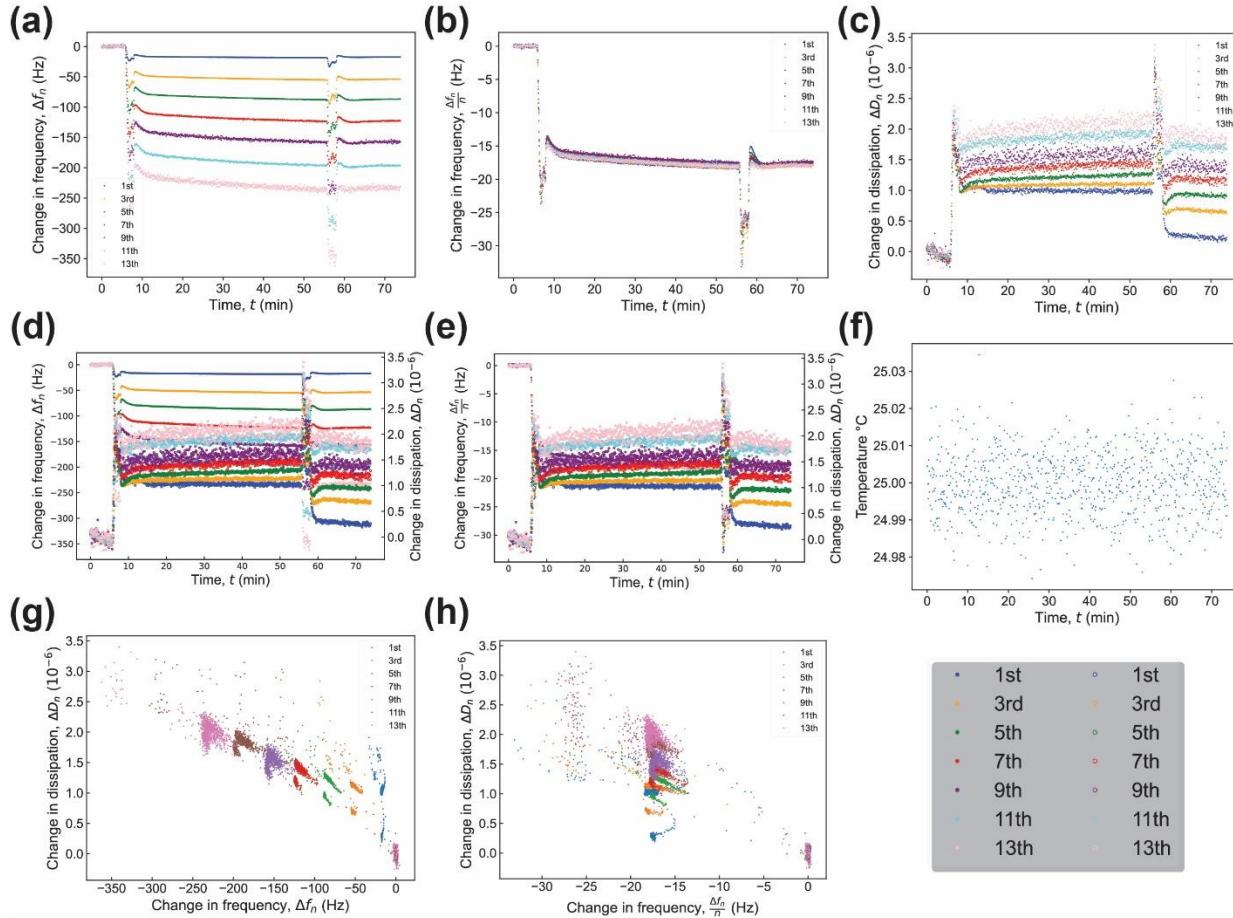


Figure 7. Raw data plots generated by BraTaDio for film formed from a solution of BSA at 1 mg/mL in PBS adsorbed to an Au-coated quartz crystal. (a) Absolute frequency  $f_n$  as a function of time  $t$ , (b) corresponding absolute dissipation  $D_n$  as a function of time for  $n = 3, 5, 7, 9, 11$ , and 13. The peaks seen in panel (b) correspond to transition periods, that is, pumping BSA after the PBS baseline was established ( $t = 5$  min), and the second to a PBS wash ( $t = 55$  min).

284 The relevant experimental data can be visualized by selecting the '*Plot shifted data*' option. For  
285 example, change in frequency as a function of time,  $\Delta f_n$  vs time  $t$ , Figure 8(a), change in  
286 normalized frequency as a function of time,  $\Delta f_n(/n)$  vs time  $t$ , Figure 8(b), change in dissipation  
287  $\Delta D_n$  vs time  $t$ , Figure 8(c), combined change in (normalized) frequency and change in dissipation  
288 as a function of time,  $\Delta f_n/n$  and  $\Delta D_n$  vs time  $t$ , Figure 8(d), combined change in normalized  
289 frequency and change in dissipation as a function of time,  $\Delta f_n/n$  and  $\Delta D_n$  vs time  $t$ , Figure 8(e),  
290 the temperature  $T$  as a function of time,  $T$  vs  $t$ , Figure 8(f), which is critical to determine any  
291 temperature effects in collected data. Finally, change in dissipation as a function of change in  
292 frequency,  $\Delta D_n$  vs  $\Delta f_n(/n)$ , Figure 8(g), and change in dissipation as a function of change in  
293 normalized frequency,  $\Delta D_n$  vs  $\Delta f_n/n$ , Figure 8(h) to obtain qualitative insights of the adsorbed film  
294 rigidity. In these plots, commonly used for assessing differences in adsorbed protein<sup>31–33</sup> or  
295 polymer films,<sup>34</sup> a small slope is indicative of a compact and more rigid film, while a higher slope  
296 is indicative of a looser and more compliant layer. Change in frequency  $\Delta f_n$  will always be plotted  
297 as normalized change in frequency  $\Delta f_n/n$  if the '*Normalize  $\Delta f$  with its respective overtone*' option  
298 is checked. The change in frequency  $\Delta f_n$  and change in dissipation  $\Delta D_n$  plots are automatically  
299 generated, and no selection is required. If one selects normalize  $\Delta f_n$  with its respective overtone  
300  $n$ , all associated  $\Delta f_n$  plots will be normalized ( $\Delta f_n/n$ ). This is not the case, however, for data used  
301 for model application purposes, as they will use normalized frequency if the model/equation  
302 requires it, regardless of the selection of this option. Note that when plotting shifted data (change  
303

304 in frequency and change in dissipation values), only the ‘*Plot shifted data*’ option with at least one  
 305 overtone must be selected.



**Figure 8. Plots generated by BraTaDio for a film formed from a solution of BSA at 1 mg/mL in PBS adsorbed to an Au-coated quartz crystal.** (a) Change in frequency  $\Delta f_n$  as a function of time  $t$ , (b) change in frequency normalized by overtone order,  $\Delta f_n/n$  as a function of time  $t$ , (c) corresponding change in dissipation  $\Delta D_n$  as a function of time, (d) change in frequency normalized by overtone order,  $\Delta f_n/n$  and corresponding change in dissipation  $\Delta D_n$  as a function of time for  $n = 5$  and  $7$  for clarity, (e) change in dissipation  $\Delta D_n$  as a function of change in frequency normalized by overtone order,  $\Delta f_n/n$ , for  $n = 3, 5$ , and  $7$  for clarity, and (f) temperature  $T$  as a function of time. Data collected with a QCM-I system.

306

### 307 3.2 Data analysis options

308 Matching QCM-D experimental data to models that provide physical interpretation is key for the  
 309 quantitative characterization of liquids interacting with the quartz crystal surfaces or nanofilms.  
 310 Models can be classified into steady-state models and kinetic models.<sup>35,36</sup> With pyQCM-BraTaDio,  
 311 it is possible to apply models of steady state (in equilibrium) thin films using one of the following  
 312 models: (i) the Sauerbrey equation for very thin films,<sup>4</sup> (ii) shear-dependent compliance of a thin

313 viscoelastic film in a Newtonian liquid,<sup>12</sup> and (iii) determination of the  
314 quartz crystal thickness.<sup>37</sup> These models are described below,  
315 accompanied with experimental examples. It is important to note that the  
316 viscoelastic properties measured via QCM-D may deviate significantly  
317 from those obtained via bulk rheometers. That is in part, due to the fact  
318 that QCM-D measures at much higher frequencies (*i.e.*, 5 – 65 MHz)  
319 than bulk rheometers (*i.e.*, 0.1 – 100 kHz),<sup>38</sup> and that the probing depth  
320 of QCM-D is of approximately 250 nm or less.<sup>2,3</sup> For more complex  
321 models, the reader is referred to a review by Johannsmann *et al.*<sup>11</sup>

### 322 3.2.1 The Sauerbrey equation for thin, rigid films

323 The Sauerbrey equation (eq 2) is a linear relationship between the resonance frequency change  
324 and the mass change of the acoustic oscillator:<sup>4,10,11</sup>

$$325 \quad \Delta m_{\text{Sauerbrey}} = -c_{\text{Theo}} \cdot \frac{\Delta f_n}{n} \quad (2)$$

326 where  $\Delta m_{\text{Sauerbrey}}$  is the change in Sauerbrey mass in (ng/cm<sup>2</sup>) (or mass per unit area),  $\Delta f_n$  is the  
327 change in frequency of overtone  $n$  in (Hz),  $n$  is the overtone order, and  $c_{\text{Theo}}$  the mass sensitivity  
328 constant in (ng/cm<sup>2</sup>·Hz).

329 The Sauerbrey equation is applicable to very thin films, with a change in mass small compared to  
330 the quartz crystal, that can be considered rigid (no deformation) and perfectly coupled to the  
331 quartz crystal surface (no slip), homogeneous and evenly distributed over the quartz crystal  
332 surface. The theoretical value of  $c_{\text{Theo}}$  for a 5 (MHz) crystal is 17.7 (ng/(cm<sup>2</sup>·Hz)). The true  $c_{\text{True}}$   
333 can be obtained from eq 3:

$$334 \quad c_{\text{True}} = \frac{\vartheta_q \cdot \rho_q}{2f_0^2} \quad (3)$$

335 Where  $\vartheta_q$  is the wave velocity in quartz,  $\rho_q$  is the density of quartz, and  $f_0$  is the measured,  
336 fundamental resonance frequency. It is frequent to report  $\Delta m_{\text{Sauerbrey}}$  for one overtone order of  
337 interest, Figure 10(a). However, more accurate  $\Delta m_{\text{Sauerbrey}}$  can be obtained from the slope of the  
338 change in frequency of each overtone  $\Delta f_n$  as a function of overtone order  $n$  and multiplying it by  
339 the mass sensitivity constant,  $c_{\text{Theo}}$ . Using the theoretical values is most of the times a good  
340 approximation, as  $c_{\text{Theo}}$  and  $c_{\text{True}}$  are usually in very good agreement. However, when the  
341 calibration values are provided, the Sauerbrey mass can be calculated using  $c_{\text{True}}$ .

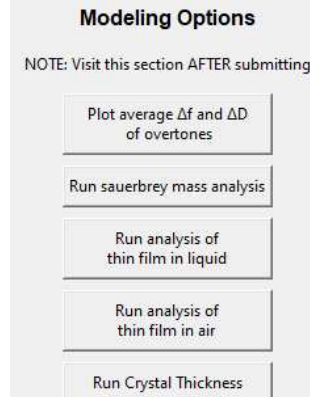


**Figure 9.** Available modelling options packaged in pyQCM-BraTaDiO.

342 The data shown in Figure 10 corresponds to the Sauerbrey mass of a BSA film after a PBS wash  
 343 formed from a 1 mg/mL bulk solution in PBS. Details are described in the *Model Experiments*  
 344 section in the SI, and plots obtained from these experiments are shown in Figures 6, 7, and 8.  
 345 pyQCM-BraTaDi plots the Sauerbrey mass for each selected overtone order, Figure 10(a) and

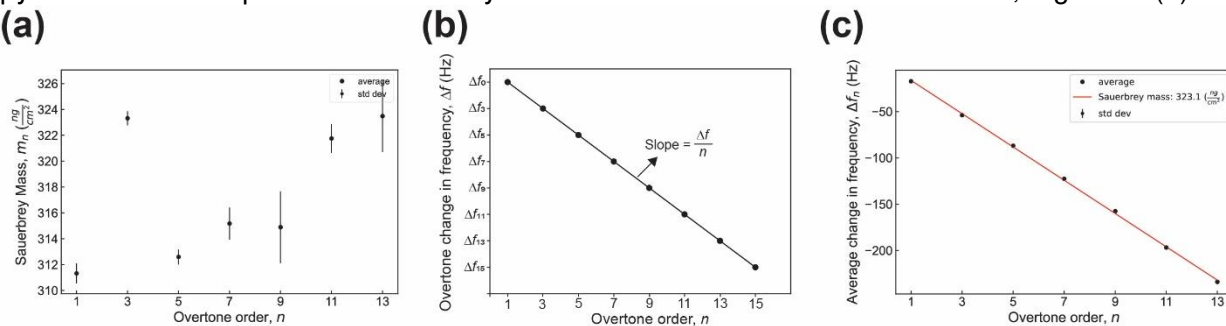


**Figure 10. Sauerbrey mass as a function of overtone order.** (a) Sauerbrey mass calculated as a function of each individual overtone order, (b) linear regression model to obtain the Sauerbrey mass using the changes in frequency from all available overtones, and (c) Sauerbrey mass calculated from performing a fit to the average change in frequency as a function of overtone order for the data range shown in Figure 6 (BSA after PBS wash).

346 saves the Sauerbrey mass values in *sauerbrey\_output.csv* file in the *selected\_ranges\_directory*.  
 347 It also plots and displays the Sauerbrey mass obtained from calculating the slope of the linear  
 348 regression and multiplying by the mass sensitivity constant  $c_{\text{True}}$ , Figure 10(c). Similar results for  
 349 an experiment conducted in a QSense system are shown in SI Figures 1, 4, and 5.

### 350 3.2.2 Shear-dependent compliance of a thin viscoelastic film in a Newtonian liquid

351 For the cases in which the film formed on the surface of the quartz sensor is significantly more  
 352 rigid than the environment Newtonian liquid, it is possible to obtain the shear-dependent  
 353 compliance of the film by plotting the change in bandwidth over the negative of the change in  
 354 frequency,  $\frac{\Delta\Gamma}{-\Delta f}$ , as a function of the overtone order,  $n$ , and calculating the slope:<sup>11,12</sup>

$$355 \frac{\Delta\Gamma}{\Delta f} \approx J'_f \omega \eta_{\text{bulk}} = J'_f 2\pi n f_0 \eta_{\text{bulk}} \quad (5)$$

356 where  $J'_f$  is the shear dependent compliance of the film,  
 357  $\omega$  the angular frequency ( $\omega = 2\pi n$ ), and  $\eta_{\text{bulk}}$  is the  
 358 viscosity of the Newtonian fluid. This equation assumes  
 359 that the viscous dependent compliance of the film is  
 360 much smaller than the shear dependent viscous  
 361 compliance of the bulk liquid,  $J''_f \ll J''_{\text{bulk}}$ . The model  
 362 was derived by Du and Johannsmann and a detailed  
 363 derivation can be found elsewhere.<sup>12</sup>

364 pyQCM-BraTaDi calculates the shear-dependent  
 365 compliance of a thin viscoelastic film in a Newtonian  
 366 liquid by computing the slope of the bandwidth shift for

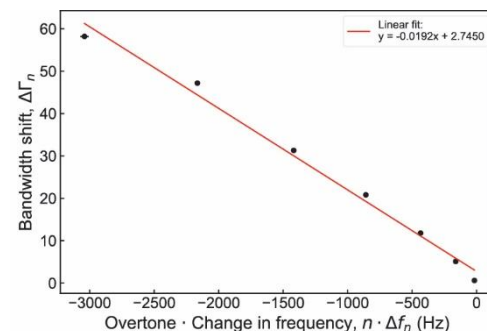


**Figure 11. Shear dependent compliance,  $J''_f$  of a BSA film formed from a bulk solution of 1 mg/mL BSA in PBS after a PBS wash.**

367 each overtone ( $\Delta f_n$ ) as a function of the change in frequency times its overtone order value ( $n \cdot$   
368  $\Delta f_n$ ). Figure 11 shows the sheard-dependent compliance of a BSA film after a PBS wash formed  
369 from a 1 mg/mL bulk solution in PBS. The calculated value  $J'_f$  is 0.0192 Pa<sup>-1</sup>. The datapoints  
370 displayed in the generated plot are saved in *thin\_film\_liquid\_output.csv* file in the *selected\_ranges*  
371 directory. Experimental details are described in the *Model Experiments* section, and plots  
372 obtained from these experiments are shown in Figures 6, 7, and 8.

### 373 3.2.3 Shear-dependent compliance of a thin viscoelastic film in air

374 For the cases in which the film on the surface of the quartz sensor is exposed to air as the medium  
375 instead of a liquid, the inertial effects of the medium become negligible. It is possible to obtain the  
376 shear-dependent compliance of the film by plotting the normalized change in frequency  $\frac{\Delta f}{n}$ , as a  
377 function of the square of the overtone order,  $n^2$ , and calculating the slope.<sup>11,24,25</sup>

378 
$$(\Delta f/n)/\Delta n^2 \approx J'_f \quad (6)$$

379 If the slope is relatively constant, it suggests that the shear-dependent compliance  $J'_f$  is relatively  
380 insensitive to the frequency.

### 381 3.2.4 Estimation of the quartz crystal thickness

382 For the cases in which the true thickness of the crystal is required, and the calibration resonance  
383 peaks known, it is possible to estimate the thickness of the crystal  $h_q$ . The implementation is  
384 based on the work by Reviakine *et al.*,<sup>37</sup>

385 
$$f_n = \frac{n}{2h_q} \sqrt{\frac{\mu_{qn}}{\rho_q}} \quad (7)$$

386 
$$\mu_{qn} = \mu_q + \frac{\epsilon}{\kappa} - \frac{8\epsilon^2}{\pi^2 n^2 \kappa} \quad (8)$$

387 where  $n$  is the overtone order,  $h_q$  is the crystal thickness,  $\rho_q$   
388 the density of quartz (2650 kg/m<sup>3</sup>),  $\mu_{qn}$  is the elastic  
389 modulus of quartz considering piezoelectric stiffening,  $\mu_q$  is  
390 the shear modulus of quartz (2.93·10<sup>10</sup> Pa),  $\epsilon$  is the  
391 piezoelectric stress coefficient (-9.24·10<sup>-2</sup> C/m<sup>2</sup>), and  $\kappa$  is  
392 the dielectric constant (3.982·10<sup>-11</sup> F/m).

393 pyQCM-BraTaDio calculates the thickness of the quartz  
394 sensor for the cases in which the calibration resonance  
395 frequency values have been provided. The corresponding  
396 outputs are a plot displaying the calculated  $h_q$  from the user  
397 defined number of overtones and saves the computed  
398 value in the *crystal\_thickness\_output.csv* file in the *selected\_ranges* directory.

## 399 4. Impact

400

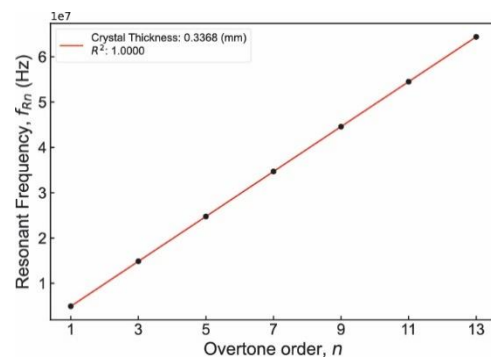


Figure 12. Determination of the quartz crystal thickness.

401 QCM-D data model applications rely on the *a priori* knowledge of various quartz crystal properties,  
402 such as fundamental resonance frequency and bandwidth,  $f_0$  and  $\Gamma_0$  respectively, higher overtone  
403 order resonance frequencies and bandwidth,  $f_n$  and  $\Gamma_n$  respectively, and theoretical mass  
404 sensitivity constant  $c_{\text{Theo}}$  (-17.7 ng/cm<sup>2</sup>·Hz at 5 MHz). For those cases in which only changes in  
405 frequency  $\Delta f_n$  and changes in dissipation  $\Delta \Gamma_n$  without offset values (e.g., data coming from a  
406 QSense system) are exported or theoretical values are not acceptable for model application  
407 purposes, it is possible to read a calibration file containing the measured resonance frequencies  
408 and bandwidths of a free oscillating crystal in air and use those values to calculate, for example,  
409 the true mass sensitivity constant  $c_{\text{True}}$  or crystal thickness  $h_{\text{crystal}}$ . Details on how to obtain  
410 calibration files from each compatible system with pyQCM-BraTaDio and how to generate/obtain  
411 a calibration are detailed in the Supporting Information.

412

## 413 **5. Conclusions**

414 pyQCM-BraTaDio is a Python software implemented *ad hoc* to expedite the process of data  
415 mining and analysis of QCM-D experimental data. We begin with a Tkinter GUI for metadata  
416 collection. These inputs and data are fed to several routines to mine and shift reformatted data  
417 with the Pandas and NumPy libraries. The user is able to interact with QCM-D in a novel way via  
418 a Matplotlib interactive plot widget towards the end of the workflow. This interaction offers the  
419 user to apply several models such as Sauerbrey, thin film in liquid, thin film in air, and crystal  
420 thickness. This tool is key for efficient data analysis in preference over laborious spreadsheet  
421 evaluation.

422

## 423 **6. Acknowledgements**

424

425 R.C.A.E. acknowledges funding from the NSF-CREST: Center for Cellular and Biomolecular  
426 Machines through the support of the National Science Foundation (NSF) Grant No. NSF-HRD-  
427 1547848. R.C.A.E. and B.P. acknowledge funding from the CAREER grant NSF CMMI Grant No.  
428 #2239665 awarded to R.C.A.E.

429

## **7. Supporting Information**

430

431 The authors have compiled additional supporting information in a separate document containing  
432 more details on the software's execution, as well as demonstrating the efficacy of the software  
433 across multiple QCM-D devices.

434

## **8. References**

435

1. Bruckenstein, S. & Shay, M. Experimental aspects of use of the quartz crystal microbalance in solution. *Electrochim. Acta* **30**, 1295–1300 (1985).
2. Easley, A. D. *et al.* A practical guide to quartz crystal microbalance with dissipation monitoring of thin polymer films. *J. Polym. Sci.* **60**, 1090–1107 (2022).
3. Levi, M. D. *et al.* In Situ Porous Structure Characterization of Electrodes for Energy Storage and Conversion by EQCM-D: a Review. *Electrochim. Acta* **232**, 271–284 (2017).
4. Sauerbrey, G. Verwendung von Schwingquarzen zur Waegung dünner Schichten und zur Mikrowaegung. *Zeitschrift fuer Physik* **155**, 206–222 (1959).
5. Lu, C.-S. & Lewis, O. Investigation of film-thickness determination by oscillating quartz resonators with large mass load. *J. Appl. Phys.* **43**, 4385–4390 (1972).

445 6. Friedt, J.-M., Choi, K. H., Frederix, F. & Campitelli, A. Simultaneous AFM and QCM  
446 Measurements. *J. Electrochem. Soc.* **150**, H229 (2003).

447 7. Borovsky, B. P., Garabedian, N. T., McAndrews, G. R., Wieser, R. J. & Burris, D. L.  
448 Integrated QCM-Microtribometry: Friction of Single-Crystal MoS<sub>2</sub> and Gold from  $\mu\text{m}/\text{s}$  to  
449 m/s. *ACS Appl. Mater. Interfaces* **11**, 40961–40969 (2019).

450 8. Bailey, L. E., Kambhampati, D., Kanazawa, K. K., Knoll, W. & Frank, C. W. Using Surface  
451 Plasmon Resonance and the Quartz Crystal Microbalance to Monitor in Situ the Interfacial  
452 Behavior of Thin Organic Films. *Langmuir* **18**, 479–489 (2002).

453 9. Levi, M. D., Daikhin, L., Aurbach, D. & Presser, V. Quartz Crystal Microbalance with  
454 Dissipation Monitoring (EQCM-D) for in-situ studies of electrodes for supercapacitors and  
455 batteries: A mini-review. *Electrochem. commun.* **67**, 16–21 (2016).

456 10. Reviakine, I., Johannsmann, D. & Richter, R. P. Hearing What You Cannot See and  
457 Visualizing What You Hear. *Anal. Chem.* **83**, 8838–8848 (2011).

458 11. Johannsmann, D., Langhoff, A. & Leppin, C. Studying Soft Interfaces with Shear Waves:  
459 Principles and Applications of the Quartz Crystal Microbalance (QCM). *Sensors* **21**, (2021).

460 12. Du, B. & Johannsmann, D. Operation of the Quartz Crystal Microbalance in Liquids:  
461 Derivation of the Elastic Compliance of a Film from the Ratio of Bandwidth Shift and  
462 Frequency Shift. *Langmuir* **20**, 2809–2812 (2004).

463 13. Johannsmann, D. *Modeling of QCM Data*.

464 14. Johannsmann, D., Mathauer, K., Wegner, G. & Knoll, W. Viscoelastic properties of thin  
465 films probed with a quartz-crystal resonator. *Phys. Rev. B Condens. Matter* **46**, 7808–7815  
466 (1992).

467 15. Johannsmann, D. Viscoelastic, mechanical, and dielectric measurements on complex  
468 samples with the quartz crystal microbalance. *Phys. Chem. Chem. Phys.* **10**, 4516–4534  
469 (2008).

470 16. Johannsmann, D. *The Quartz Crystal Microbalance in Soft Matter Research. Fundamentals  
471 and Modeling*. (Springer).

472 17. Johannsmann, D. Viscoelastic Analysis of Organic Thin Films on Quartz Resonators.  
473 *Macromol. Chem. Phys.* doi:10.1002/(SICI)1521-3935(19990301)200:3.

474 18. Domack, A., Prucker, O., Rühe, J. & Johannsmann, D. Swelling of a polymer brush probed  
475 with a quartz crystal resonator. *Phys. Rev. E Stat. Phys. Plasmas Fluids Relat. Interdiscip.  
476 Topics* **56**, 680–689 (1997).

477 19. Johannsmann, D., Reviakine, I. & Richter, R. P. Dissipation in films of adsorbed  
478 nanospheres studied by quartz crystal microbalance (QCM). *Anal. Chem.* **81**, 8167–8176  
479 (2009).

480 20. Tellechea, E., Johannsmann, D., Steinmetz, N. F., Richter, R. P. & Reviakine, I. Model-  
481 independent analysis of QCM data on colloidal particle adsorption. *Langmuir* **25**, 5177–  
482 5184 (2009).

483 21. Keiji Kanazawa, K. & Gordon, J. G. The oscillation frequency of a quartz resonator in  
484 contact with liquid. *Anal. Chim. Acta* **175**, 99–105 (1985).

485 22. Kanazawa, K. K. & Gordon, J. G. Frequency of a Quartz Microbalance in Contact with  
486 Liquid. *Anal. Chem.* **57**, 1770–1771 (1985).

487 23. Voinova, M. V., Rodahl, M., Jonson, M. & Kasemo, B. Viscoelastic Acoustic Response of  
488 Layered Polymer Films at Fluid-Solid Interfaces: Continuum Mechanics Approach. *Physica  
489 Scripta* **59**, 391–396 (1999).

490 24. Shull, K. R., Taghon, M. & Wang, Q. Investigations of the high-frequency dynamic  
491 properties of polymeric systems with quartz crystal resonators. *Biointerphases* **15**, 021012  
492 (2020).

493 25. Johannsmann, D., Langhoff, A., Leppin, C., Reviakine, I. & Maan, A. M. C. Effect of Noise  
494 on Determining Ultrathin-Film Parameters from QCM-D Data with the Viscoelastic Model.  
495 *Sensors* **23**, (2023).

496 26. Mc Kinney, W. Data Structures for Statistical Computing in Python. in *Proceedings of the*  
497 *9th Python in Science Conference* (ed. van der Walt and Jarrod Millman, S.) 56–61 (2010).  
498 27. Harris, C. R. *et al.* Array programming with NumPy. *Nature* **585**, 357–362 (2020).  
499 28. Lundh, F. An introduction to tkinter. *URL: www. pythonware.*  
500 *com/library/tkinter/introduction/index. htm*.  
501 29. Thiruvathukal, E. G. K. & Läufer, K. Matplotlib: A 2D Graphics Environment. *Scientific*  
502 *Programming* **9**, 90–95 (2007).  
503 30. Virtanen, P. *et al.* SciPy 1.0: fundamental algorithms for scientific computing in Python. *Nat.*  
504 *Methods* **17**, 261–272 (2020).  
505 31. Feiler, A. A., Sahlholm, A., Sandberg, T. & Caldwell, K. D. Adsorption and viscoelastic  
506 properties of fractionated mucin (BSM) and bovine serum albumin (BSA) studied with  
507 quartz crystal microbalance (QCM-D). *J. Colloid Interface Sci.* **315**, 475–481 (2007).  
508 32. Kushiro, K., Lee, C. H. & Takai, M. Simultaneous characterization of protein-material and  
509 cell-protein interactions using dynamic QCM-D analysis on SAM surfaces. *Biomaterials*  
510 *Science* **4**, 989–997 (2016).  
511 33. Lin, J. H. *et al.* Effect of surface potential on extracellular matrix protein adsorption.  
512 *Langmuir* **30**, 10328–10335 (2014).  
513 34. Liu, G. & Zhang, G. *QCM-D Studies on Polymer Behavior at Interfaces*. (Springer Berlin  
514 Heidelberg).  
515 35. Wittmer, C. R. & Van Tassel, P. R. Probing adsorbed fibronectin layer structure by kinetic  
516 analysis of monoclonal antibody binding. *Colloids Surf. B Biointerfaces* **41**, 103–109 (2005).  
517 36. Antosiewicz, A., Senkara, E. & Cieśla, J. Quartz crystal microbalance with dissipation and  
518 microscale thermophoresis as tools for investigation of protein complex formation between  
519 thymidylate synthesis cycle enzymes. *Biosensors and Bioelectronics* **64**, 36–42 (2015).  
520 37. Reviakinea, I., Morozov, A. N. & Rossetti, F. F. Effects of finite crystal size in the quartz  
521 crystal microbalance with dissipation measurement system: Implications for data analysis.  
522 *Journal of Applied Physics* **95**, 7712–7716 (2004).  
523 38. Schroyen, B., Vlassopoulos, D., Van Puyvelde, P. & Vermant, J. Bulk rheometry at high  
524 frequencies: a review of experimental approaches. *Rheol. Acta* **59**, 1–22 (2020).